Kovács, L. L., Stépán, G., Dynamics of digital force control applied in rehabilitation robotics, *Meccanica* **38** (2003) 213-226.

Dynamics of digital force control applied in rehabilitation robotics

LÁSZLÓ L. KOVÁCS and GÁBOR STÉPÁN (stepan@mm.bme.hu)*
Department of Applied Mechanics, Budapest University of Technology and Economics, H-1521 Budapest, Hungary; Tel.: +36 1 463 1369, Fax: +36 1 463 3471

Abstract. Controlled structures are often required to keep desired contact forces between some of its elements. A classical example is the controlled interaction of a robot with its environment when the control of the contact force between the robotic actuator and the work-piece is prescribed. Experiments often call the attention to the destabilizing digital effects, like sampling, in these systems. In this paper the stability of a newly developed force based teaching-in method is analysed. The method is applied in rehabilitation robotics. The stability limits are presented in the parameter space of the sampling time, control gains and mechanical parameters of the robot. The least force error and the fastest settling force signal are calculated. The influence of the elasticity of the force sensor is analysed as well as the possible bifurcations. Real parameter case study confirms the analytical predictions.

Key words: Nonlinear control, Sampling effect, Stability, Rehabilitation robotics, Biomechanics.

1 Introduction

One of a recently started research project of the European Union (REHAROB IST-1999-13109) aims to provide personalised, three-dimensional upper limb motion therapy for the disabled and for patients suffering from spastic hemiparesis, which mostly arises as a consequence of stroke or other brain injuries.

Similar research projects have developed physiotherapy machines for upper limb rehabilitation after a stroke in North-America [1], [2], [3], and there are also some commercial applications [4] and patents [5] there. The commercialisation of the laboratory results of European researches [6], [7], [8] practically failed due to the unique production requirements of the elements of the corresponding physiotherapy machines. The medical certification of these machines is one of the major obstacles of commercialisation.

The REHAROB project declares that the key to the success of commercialisation is the use of commercial sub-systems. In this project – and later in the commercialised REHAROB cell – the therapy will be driven by two

* This e-mail address is available for all problems and questions.

co-operating industrial robots, using force/torque (F/T) measurement for programming by demonstration (teaching-in). For safety, certification, and economic reasons, standard industrial robots are used with standard six degree-of-freedom (DOF) F/T transducers at each orthosis (a device that holds the upper and lower arms during therapy).

In order to provide adequate safety, the REHAROB cell will include 6 DOF F/T transducers mounted between the outer shell of the orthosis and its inner shell attached to the patient's arm (see F/T transducer#1 in Figure 1). The primary task of this F/T sensor is to record the reference force/torque values during teaching-in, which will serve as a threshold value to trig the emergency stop signal during physiotherapy.

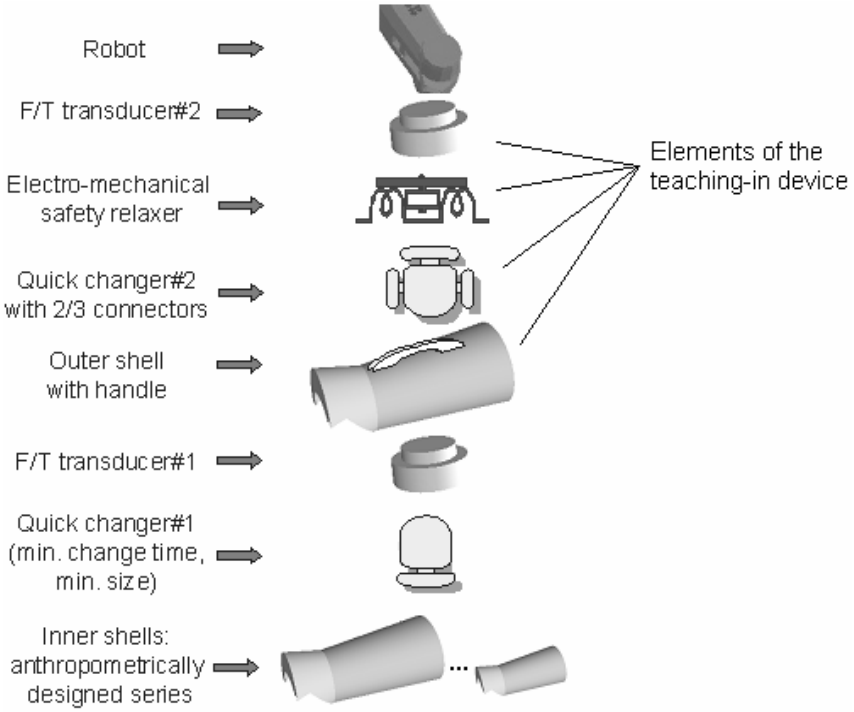

Figure 1 Structure of the REHAROB engineered orthosis

Another 6 DOF F/T transducer has to be used to get the force signal for the digital force control, i.e. to achieve that the end effector of the robot always move in a way that the desired force and torque are zero at the F/T transducer#2 (see Figure 1). In other words, the position and orientation data of the robot is to be recorded during the exercises carried out by the physiotherapist, while the F/T transducers are continuously relaxed by the robots' movements corresponding to an appropriate force control-law.

Due to the application of commercial elements in the above system, the overall sampling time and the corresponding time delay is greater than the usual values in case of a single position controlled industrial robot. The low sampling rate in the outer force control loop of this hierarchic control strategy causes serious stability problems. The specialist literature often calls the attention to the destabilising digital effects in force control either qualitatively (see, for example, Raibert and Craig [9], Craig [10]), or in analytical form for 1 DOF mechanical models (see Whitney [11], [12]). In this paper, we give analytical results presented in the form of stability charts. These charts support the development of these robots at the design stage where both mechanical and control parameters can still be varied.

The subsequent sections of this paper describe the basic concept of a simplified, 2 DOF model of the teaching-in device (see marked elements of the engineered orthosis in Figure 1), and the stability analysis of a discrete mathematical model of the above described digital force control. Then a stability chart is presented in the plane of mechanical and control parameters and also the nature of the loss of stability is investigated. At the end, a real parameter case study confirms the analytical predictions.

2 Mechanical models of force control

A uni-directional model of the robotic structure is presented in this section. The first approach gives a continuous model for the force control, while the more sophisticated model involves the digital effects, too.

2.1 Continuous model

To construct an appropriate control strategy, and also for the better physical understanding of the technical phenomenon, we consider a simplified one-dimensional model of the coupled human-machine system, which still has three mechanical degree-of-freedom. The following subsystems are connected in a serial way in the single dimension described in the model (see Figure 2).

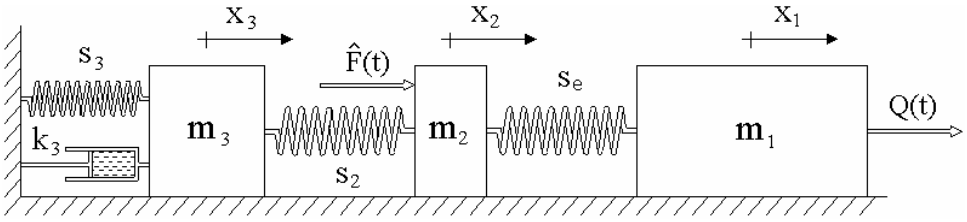

Figure 2 The 3 DOF model of the human-machine coupled system

The spring, the dashpot and the block with subscripts 3 model the elasticity, damping and the inertial effects of the upper arm; the second block between two springs refers to the inertia of the outer shell of the orthosis, that of the quick changer and the electromechanical safety relaxer between the two F/T transducers; the third block with subscript 1 represents the inertia of the robotic arm itself. The forces $\hat{F}(t)$ and $Q(t)$ denote the forces applied by the physiotherapist and the unknown control force commanded by the standard robot controller, respectively.

From the viewpoint of the force control, the effect of the human body and other elements between the arm and the outer shell of the orthosis are negligible, since the force applied by the therapist at the outer shell of the orthosis compensates the patient's resistance. Thus, it is enough to investigate a 2 DOF oscillatory system to construct a proper control-law that provides the desired zero force and torque at the tool-centre-point (TCP) of the robot end effector.

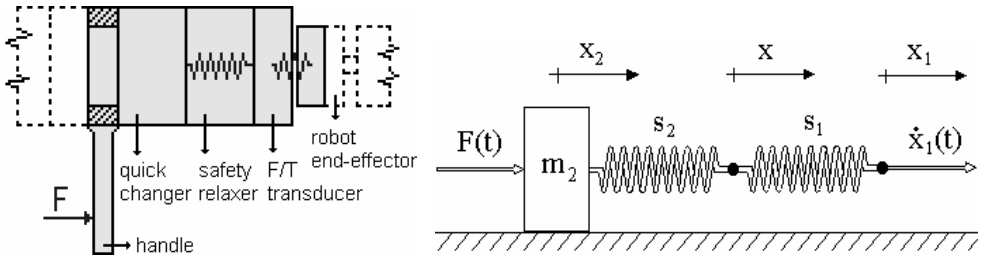

Figure 3 The mechanical model of the robot teaching-in problem

Figure 3 presents a simplified model of the teaching-in device described in the previous paragraph, where m_2 denotes the total mass of the handle, the quick changer and a portion of the safety relaxer, while s_1 and s_2 denote the stiffness of the F/T transducer and the compliant safety relaxer, respectively. The excitation force F means the force that has to be exerted by the therapist to provide the desired motion of the teaching-in device during programming by demonstration in addition to the force $\hat{F} - F$ applied for the patient's arm. In an ideal case, this additional force F is very small compared to the regular forces used during the therapy. The position of the TCP is denoted by x_1, while $\dot{x}_1$ is its velocity. This velocity is determined through a kinematic constraint as proposed in Stépán and Haller [13].

The control law envisaged here considers that the stiffness of the applied industrial F/T transducer is higher with three orders of magnitude than the stiffness of the compliant safety relaxer. Thus, the displacement x of the common joint of the springs s_1 and s_2 can be estimated by x_1, and the resultant stiffness of the serially connected springs is approximately s_2. The control law and the equation of motion of the teaching-in device yield the continuous mechanical model, as follows:

$$\dot{x}_1 = -k_p s_2(x_1 - x_2) + \dot{x}_2 \ , \tag{1}$$

$$m_2 \ddot{x}_2 = s_2(x_1 - x_2) + F(t) \ . \tag{2}$$

Clearly, this provides asymptotic stability for the force error $s_2(x_1 - x_2)$ for any positive proportional control gain k_p in analogue control systems. While this linear model provides global stability properties, the unmodelled non-linear effects – like saturation at the actuators or non-linear spring characteristics at the force sensors or round-off errors at the processors – may result in local stability properties in practical cases [14].

2.2 Discrete model

In the REHAROB project, a standard industrial robot controller with digital position/velocity control will be used. The digital version of the control presented as the kinematic constraint (1) is modelled with periodic sampling and a zero-order-holder (ZOH) as shown in Figure 4. The digital processor samples the force signal at the time instants $t_j = j\tau, \ \ j = 0,1,2,\ldots$, where τ stands for the sampling time and the ZOH transforms the impulse sequence of the desired velocities into a piecewise constant excitation.

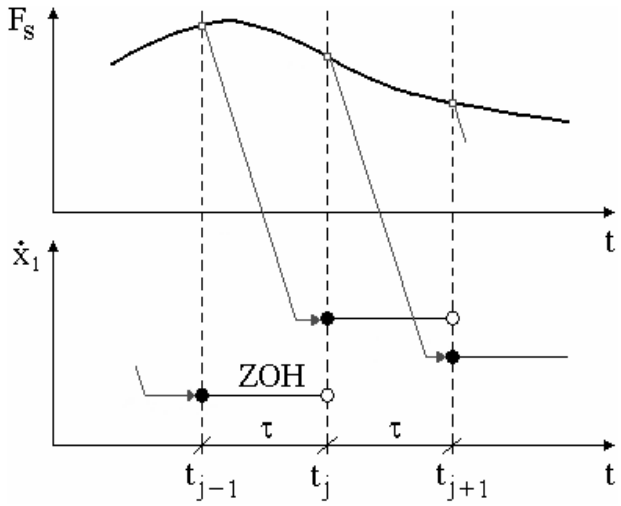

Figure 4 The sampled kinematic constraint

Thus, the commanded velocity – determined through the discretised kinematic constraint – is calculated from the force signal sampled at the beginning of the previous sampling interval:

$$\dot{x}_1(t) = -k_p s_2 \big(x_1(t_j - \tau) - x_2(t_j - \tau)\big) + \dot{x}_2(t_j - \tau)\,, \qquad t \in [t_j, t_j + \tau)\ . \tag{3}$$

The equation of motion of the teaching-in device has the form:

$$m_2 \ddot{x}_2(t) = s_2 \big(x_1(t) - x_2(t)\big) + F(t)\ . \tag{4}$$

Introducing a new convenient state vector $\mathbf{y} = \mathrm{col}(\ x_1 - x_2 \quad \dot{x}_2\ )$, equations (3) and (4) can be arranged in matrix form:

$$\dot{\mathbf{y}}(t) + \begin{pmatrix} 0 & 1 \\ -\omega_n^2 & 0 \end{pmatrix} \mathbf{y}(t) = \begin{pmatrix} -k_p s_2 & 1 \\ 0 & 0 \end{pmatrix} \mathbf{y}(t_j - \tau) + \begin{pmatrix} 0 \\ F(t) \end{pmatrix}, \qquad t \in [t_j, t_j + \tau)\ , \tag{5}$$

where $\omega_n = \sqrt{s_2 / m_2}$ is the natural angular frequency of the uncontrolled system.

3 Force error of the robot

To estimate the force error ("resistance") of the robot, a constant force $F(t) \equiv F_0$ is applied which leads to a constant acceleration *a* after the transient motion. In this case, the mean time delay τ_m with respect to the velocity $\dot{x}_2$ is 1.5τ (see Figure 5).

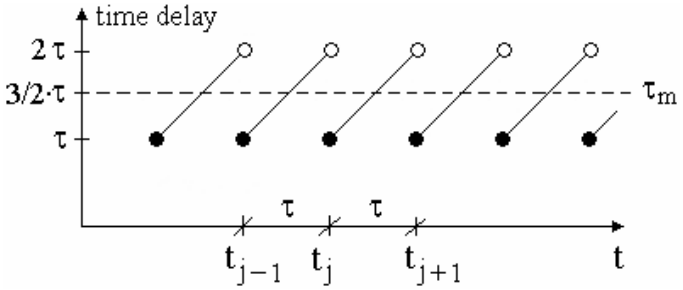

Figure 5 The mean time delay

The force error, which inevitably loads the therapist, will be the constant $\Delta F = s_2(x_1 - x_2)$ after a transient. For the stationary case, equations (3) and (4) yield:

$$at = -k_p \Delta F + a(t - 3\tau/2) \quad \text{and} \quad m_2 a = F_0 + \Delta F \tag{6}$$

from which, the force error ratio is:

$$\left|\frac{\Delta F}{F_0}\right| = \frac{3\tau}{2k_p m_2 + 3\tau} \ . \tag{7}$$

The greater the proportional gain is, the smaller the force error becomes. When the proportional gain is zero, i.e. the control is switched off, the robot does not move at all. This means that the robot arm stays in equilibrium and so the force error is just equal and opposite to the force applied by the physiotherapist. Negative gain values have no practical meaning since the robot will move opposite to the direction the therapist would like to achieve.

4 Stability analysis

It is well known that force controlled robots tend to lose robustness or even stability depending on the environment they are in contact with. Experiments often call the attention to the destabilizing digital effects, like sampling, in these systems. A discrete mathematical model is constructed and analysed in order to obtain a clear picture about the stability properties of the above mechanical model.

4.1 Discrete mapping

For the stability analysis, we consider constant, or without loss of generality, zero external force: $F(t) \equiv F_0 = 0$. Referring to Stépán [15], the stability investigation of the trivial solution of the piecewise continuous system (5) is carried out via the analytical construction of a discrete mapping. The non-homogeneous ordinary differential equation (5) has a piecewise constant right-hand side; the general solution for each sampling interval can be constructed from the sum of the general solution of the homogeneous part and a particular (actually, constant) solution of the non-homogeneous part:

$$\mathbf{y}(t) = \begin{pmatrix} \cos\omega_n t & \sin\omega_n t \\ \omega_n \sin\omega_n t & -\omega_n \cos\omega_n t \end{pmatrix} \begin{pmatrix} A \\ B \end{pmatrix} + \begin{pmatrix} 0 \\ v_j \end{pmatrix}, \qquad t \in [t_j, t_{j+1}) \tag{8}$$

where

$$v_j = -k_p s_2 y_1(t_j - \tau) + y_2(t_j - \tau) \tag{9}$$

is the constant velocity of the TCP during the *j*th sampling interval, and the parameters *A* and *B* depend on the initial conditions for the same sampling interval. Thus, the substitution of the initial conditions $\mathbf{y}(t_j)$ in Eq. (8) determine the linear system of algebraic equations:

$$\begin{pmatrix} \cos\omega_n t_j & \sin\omega_n t_j \\ \omega_n \sin\omega_n t_j & -\omega_n \cos\omega_n t_j \end{pmatrix} \begin{pmatrix} A \\ B \end{pmatrix} = \begin{pmatrix} y_1(t_j) \\ y_2(t_j) - v_j \end{pmatrix} . \tag{10}$$

The solution

$$A = \cos(\omega_n t_j) y_1(t_j) + \frac{\sin(\omega_n t_j)}{\omega_n} \left(y_2(t_j) - v_j \right) , \tag{11}$$

$$B = \sin(\omega_n t_j) y_1(t_j) - \frac{\cos(\omega_n t_j)}{\omega_n} \left(y_2(t_j) - v_j \right) \tag{12}$$

give the unknown coefficients A and B in Eq. (8). Clearly, the elements of the state variable $\mathbf{y}$ can be calculated at the end of the jth sampling interval by substituting $t = t_j + \tau$ into Eq. (8). After some trigonometric transformation, the substitution of (11) and (12) results

$$y_1(t_j + \tau) = \cos(\omega_n \tau) y_1(t_j) - \frac{1}{\omega_n} \sin(\omega_n \tau) y_2(t_j) + \frac{1}{\omega_n} \sin(\omega_n \tau) v_j , \tag{13}$$

$$y_2(t_j + \tau) = \omega_n \sin(\omega_n \tau) y_1(t_j) + \cos(\omega_n \tau) y_2(t_j) + \left(1 - \cos(\omega_n \tau)\right) v_j . \tag{14}$$

This can also be arranged in matrix form if the 3 dimensional discrete state vector

$$\mathbf{z}_j = \begin{pmatrix} y_1(t_j) \\ y_2(t_j) \\ v_j \end{pmatrix} , \qquad j = 1,2,\ldots \tag{15}$$

is introduced. The coefficient matrix $\mathbf{A}$ of the three dimensional linear mapping

$$\mathbf{z}_{j+1} = \mathbf{A}\, \mathbf{z}_j \tag{16}$$

can be constructed from the coefficients of the corresponding terms of formulae (13), (14) and (9) as follows:

$$\mathbf{A} = \begin{pmatrix} \cos(\omega_n\tau) & -\frac{1}{\omega_n}\sin(\omega_n\tau) & \frac{1}{\omega_n}\sin(\omega_n\tau) \\ \omega_n \sin(\omega_n\tau) & \cos(\omega_n\tau) & 1-\cos(\omega_n\tau) \\ -k_p s_2 & 1 & 0 \end{pmatrix}. \tag{17}$$

4.2 Convergence

The map (17) describes the connection between the state variables at consecutive sampling instants. The trivial solution of this linear mapping corresponds to the constant (or zero) force error in our model (3) and (4), or (5). Referring to Kuo [16], the trivial solution is stable, if and only if all the eigenvalues $\mu_{1,2,3}$ of the principal matrix **A** in Eq. (17) are located in the unit disc of the complex plane.

Substitution of the usual exponential trial solution

$$\mathbf{z}(t) = \mathbf{K}e^{\lambda t},\ \mathbf{K} \in \mathbf{R}^3 \tag{18}$$

into the three dimensional linear mapping (16) yields the characteristic equation:

$$(\mathbf{I} - \mathbf{A}e^{-\lambda\tau})\,\mathbf{K} = 0,\ \mathbf{K} \neq 0 \quad \Rightarrow \quad \det(\mathbf{I} - \mathbf{A}e^{-\lambda\tau}) = 0 \tag{19}$$

where the characteristic roots λ_k, $k = 1,2,\ldots$ have to be located in the left half of the complex plane to provide stability as it follows from Eq. (18). Then, introducing a new complex variable, the so-called characteristic multiplier μ by

$$\mu = e^{\lambda\tau} \quad \Rightarrow \quad \{\, \mathrm{Re}\,\lambda_j \le 0, \quad j = 1,2,\ldots \quad \Leftrightarrow \quad |\mu_{1,2,3}| \le 1 \,\} \tag{20}$$

the stability condition $|\mu_{1,2,3}| \le 1$ yields. This is just the condition quoted above from Kuo [16]. Thus, the stability of the trivial solution of the map (16) can be investigated by means the characteristic equation of the principal matrix **A**:

$$\det(\mu\mathbf{I} - \mathbf{A}) = 0\ . \tag{21}$$

This can be factorised. The free translation of the system is described by the characteristic root $\lambda = 0$, i.e., $\mu = 1$ is the corresponding characteristic multiplier that always satisfies the above equation – as it does, indeed. Introduce the new dimensionless gain and frequency parameters

$$p = k_p s_2 / \omega_n \qquad \text{and} \qquad \gamma = \omega_n \tau \ , \tag{22}$$

where γcan also be thought of as a dimensionless delay in the system. With these, the characteristic equation of the coefficient matrix **A** assumes the simple form of

$$(\mu - 1)\sum_{k=0}^{2} b_k \mu^k = (\mu - 1)\left(\mu^2 + (1 - 2\cos\gamma)\mu + 1 - \cos\gamma + p\sin\gamma\right) = 0 \ . \tag{23}$$

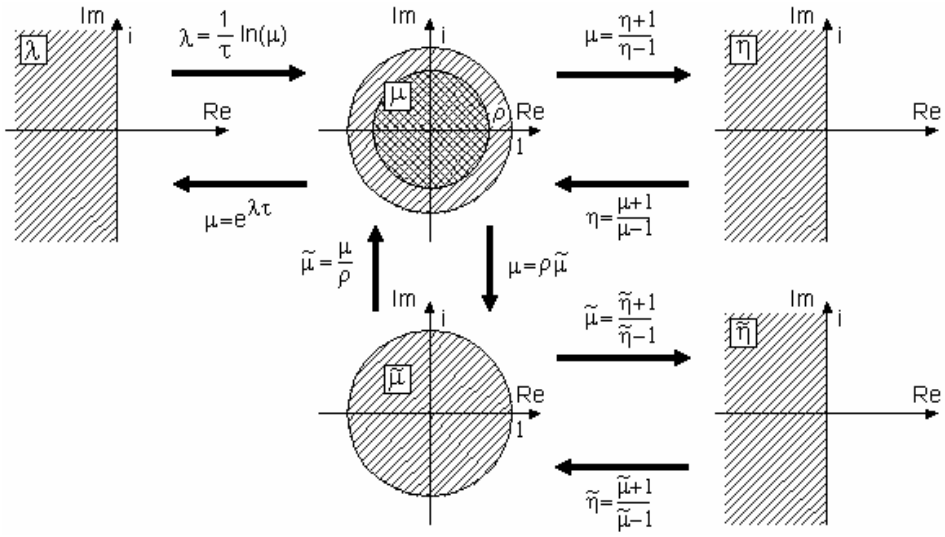

Figure 6 Transformations for stability analysis

The second-degree factor of the polynomial in (23) is investigated by the so-called Moebius transformation

$$\mu = \frac{\eta + 1}{\eta - 1} \quad \text{or} \quad \eta = \frac{\mu + 1}{\mu - 1} \ . \tag{24}$$

This transforms the unit disc into the left half of the complex plane as shown in Figure 6. Then the stability condition can be checked by the well-known Routh-Hurwitz criterion applied to the transformed polynomial equation

$$a_2 \eta^2 + a_1 \eta + a_0 = 0 \ . \tag{25}$$

The coefficients a_k can easily be calculated directly from the coefficients b_k of the Eq. (23) as:

$$\begin{pmatrix} a_2 \\ a_1 \\ a_0 \end{pmatrix} = \begin{pmatrix} 1 & 1 & 1 \\ 2 & 0 & -2 \\ 1 & -1 & 1 \end{pmatrix} \begin{pmatrix} b_2 \\ b_1 \\ b_0 \end{pmatrix} = \begin{pmatrix} 3-3\cos\gamma + p\sin\gamma \\ 2(\cos\gamma - p\sin\gamma) \\ 1+\cos\gamma + p\sin\gamma \end{pmatrix}, \tag{26}$$

where the transformation matrix is derived from the definition (24) of the Moebius transformation. The above described analytical stability investigation is also referred to as Jury's criterion (see Kuo [16]). Thus, the necessary and sufficient condition of stability is that all the coefficients (26) in Eq. (25) are positive (see Farkas [17]).

4.3 Stability chart

The positiveness of the coefficients a_k, $k = 0, 1, 2$ in (26) depends on the two parameters p and γ only. This provides the possibility to construct a two-dimensional stability chart that shows all the different kinds of possible vibrations in a single parameter plane of the dimensionless variables.

Considering formulae (26) of the coefficients, the following stability conditions are obtained:

$$\begin{aligned} a_2 > 0 \quad &\Leftrightarrow \quad p > \frac{-3+3\cos\gamma}{\sin\gamma}, \\ a_1 > 0 \quad &\Leftrightarrow \quad p < \frac{1}{\tan\gamma}, \\ a_0 > 0 \quad &\Leftrightarrow \quad p > -\frac{1+\cos\gamma}{\sin\gamma}. \end{aligned} \tag{27}$$

Figure 7 shows the corresponding stable domain in the parameter plane, and presents also the bifurcations, which may occur along the boundaries.

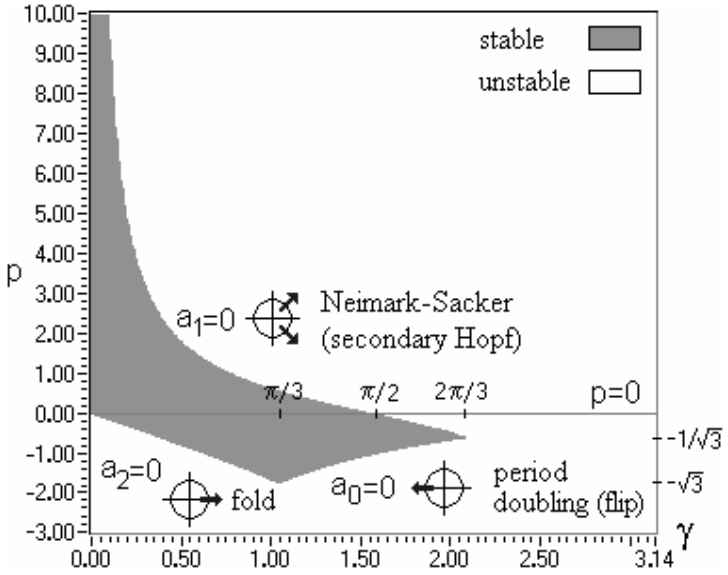

Figure 7 Stability chart: the stability boundaries a_i=0 and the shaded stable domain

5 Dynamic properties

In the above stability chart, the frequency of the vibrations occurring along the secondary Hopf bifurcation can be estimated, and also the strongest exponential decay, the fastest settling signal, can be calculated.

5.1 Bifurcations

The stability chart shown in Figure 7 has different types of stability boundaries where different kinds of bifurcations occur. Although, all the three possible bifurcations of discrete systems can be found along the stability limits, the typical one is the Neimark-Sacker bifurcation in practical cases. This bifurcation is topologically equivalent to the Hopf bifurcation of autonomous systems. Thus, it occurs when the roots of Eq. (23) have the complex conjugate form $\mu_{2,3} = \cos\alpha \pm i\sin\alpha,\ \alpha \in (0,\pi)$ along the corresponding stability limit. As it follows from the characteristic multipliers

$$\mu_1 = 1 \quad \text{and} \quad \mu_{2,3} = -\frac{1-2\cos\gamma}{2} \pm \frac{1}{2}\sqrt{4\cos\gamma^2 - 4p\sin\gamma - 3} \tag{28}$$

calculated from Eq. (23), the Neimark-Sacker bifurcation occurs along the stability limit a_1=0 if the condition

$$p > \frac{4\cos\gamma^2 - 3}{4\sin\gamma} \tag{29}$$

is also satisfied (see Figure 8).

The other two kinds of bifurcation are the period doubling (flip) and the fold (saddle-node) bifurcations along the stability limits a_0=0 and a_2=0, respectively. In these cases the proportional gain is smaller than zero, and the system moves opposite to the desired direction. These kinds of motions have theoretical importance only. When the period doubling bifurcation occurs, the arising oscillation has the period 2τ, i.e., double of the sampling time. In case of the fold bifurcation, the arising vibration has the frequency of the sampling.

5.2 Vibration frequencies

In case of the Neimark-Sacker bifurcation, the lowest frequency of the oscillation arising at the loss of stability can be calculated in closed form. The substitution of the corresponding transformed complex variables $\eta = \pm \mathrm{i}\beta$ into Eq. (25) results the linear system of equations

$$a_1\beta = 2(\cos\gamma - p\sin\gamma)\beta = 0 \ , \tag{30}$$

$$-a_2\beta^2 + a_0 = -(3 - 3\cos\gamma + p\sin\gamma)\beta^2 + 1 + \cos\gamma + p\sin\gamma = 0 \ . \tag{31}$$

The elimination of *p* results

$$\beta = \sqrt{\frac{1 + 2\cos\gamma}{3 - 2\cos\gamma}} \ . \tag{32}$$

Thus, dimensionless vibration frequency ω is obtained via the transformation of this result back to the critical characteristic roots:

$$\lambda_{1,2} = \pm \mathrm{i}\omega = \mp \ln\frac{\mathrm{i}\beta + 1}{\mathrm{i}\beta - 1} = \pm \mathrm{i}(\pi - 2\,\mathrm{atn}\,\beta) \ . \tag{33}$$

These frequencies are shown in Figure 8, and the corresponding frequency in Hz can be calculated as $f = \omega/(2\pi\tau)$. This means that the frequency of the self-excited vibration is between one sixth and one half of the sampling frequency $1/\tau$.

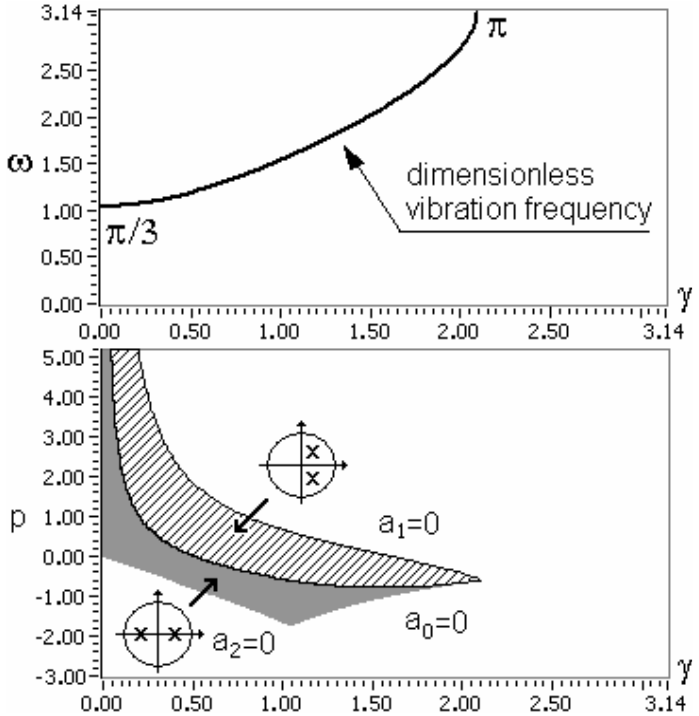

Figure 8 Complex characteristic multipliers and the corresponding vibration frequencies

5.3 Exponential decay

There are several viewpoints the engineer should consider during the design of a force-controlled structure. In the case of the rehabilitation robot, the minimum force error, that is, the less resistance against the therapist's action, requires as high gains within the stability limit, as possible. This force error can be zero theoretically, as the gain p can be increased without any upper limit in case of arbitrarily small γ, that is, for arbitrarily small sampling time τ or for ideally soft safety relaxer with $\omega_n \to 0$ (see Figure 7 and Eq. (7)). The other important point of view in the design work could be to have short transient vibrations.

According to Figure 6, it is obvious that the fastest settling force signal can be calculated by searching the minimum of the spectral radius ρ of the characteristic multipliers $\mu_{2,3}$. Thus,

$$\mu = \rho\tilde{\mu}, \quad \tilde{\mu} = \frac{\tilde{\eta}+1}{\tilde{\eta}-1} \quad \Rightarrow \quad \{|\mu| < \rho \quad \Leftrightarrow \quad |\tilde{\mu}| < 1 \quad \Leftrightarrow \quad \mathrm{Re}\,\tilde{\eta} < 0\} \qquad (34)$$

and the same algorithm described in section *4.2* results the polynomial in Eq. (25) with the following coefficients:

$$\begin{pmatrix}\tilde{a}_2\\ \tilde{a}_1\\ \tilde{a}_0\end{pmatrix}=\begin{pmatrix}1 & 1 & 1\\ 2 & 0 & -2\\ 1 & -1 & 1\end{pmatrix}\begin{pmatrix}\rho^2 b_2\\ \rho b_1\\ b_0\end{pmatrix}=\begin{pmatrix}\rho^2+(1-2\cos\gamma)\rho+1-\cos\gamma+p\sin\gamma\\ 2(\rho^2-1+\cos\gamma-p\sin\gamma)\\ \rho^2-(1-2\cos\gamma)\rho+1-\cos\gamma+p\sin\gamma\end{pmatrix}. \quad (35)$$

When ρ decreases, the stable domain bordered by $\tilde{a}_j = 0$, $j = 0,1,2$ shrinks. It shrinks to a point, when the spectral radius is $\rho = 0$, i.e., when the characteristic multipliers are $\mu_{2,3} = 0$. Thus, the dimensionless gain and frequency providing the shortest transient are obtained from Eq. (28):

$$\rho = 0 \quad \Leftrightarrow \quad \mu_{2,3} = 0 \qquad \Rightarrow \qquad \gamma = \frac{\pi}{3}, \quad p = -\frac{1}{\sqrt{3}} \ . \quad (36)$$

Physically, it means that the mapping (17) yields the desired zero force at the F/T transducers in two sampling steps only (deadbeat control). Still, this parameter setting has no practical meaning because of the negativeness of the gain parameter.

6 Real parameter case study

The physical parameter values of the mechanical model are taken from the real robotic structure:

$$\begin{aligned} s_1 &= 3.7\cdot 10^6\,[\mathrm{N/m}] & m_2 &= 3\,[\mathrm{kg}]\\ s_2 &= 1200\,[\mathrm{N/m}] & \tau &= 0.03\,[\mathrm{s}] \end{aligned} \ . \quad (37)$$

According to the stability limit a_1=0 in Figure 7, the necessary condition for the stiffness is satisfied:

$$1200\,[\mathrm{N/m}] = s_2 \approx s_e = \frac{s_1 s_2}{s_1 + s_2} < m_2 \frac{\pi^2}{4\tau^2} = 8200\,[\mathrm{N/m}] \ . \quad (38)$$

Thus, for the control gain, we have the criterion:

$$0 < k_p < \frac{\omega_n}{s_2 \tan\gamma} = 0.024\,[\mathrm{s/kg}] \ , \quad (39)$$

while the force error ratio can be estimated from below by:

$$\left|\frac{\Delta F}{F_0}\right| > \frac{3\tau}{2k_p m_2 + 3\tau} = 0.4 \ . \tag{40}$$

Choosing an appropriate control gain $k_p = 0.01$ according to the criterion (39) and applying the constant force $F_0 = 5\,[\mathrm{N}]$, the force error ratio from (7) is $|\Delta F / F_0| = 0.6$. The calculated 'resistance' of the robot during teaching-in and also its predicted stability behaviour are confirmed by the simulation results shown in Figure 9. Simulation tool was developed in LabVIEW® for the numerical solution of equations (3) and (4) with $F(t) \equiv F_0$.

As the result in Figure 9 shows, the force error tends to $-0.6F_0 = -3\ [\mathrm{N}]$, and it goes back to zero when the external force disappears. Physically, this means that the physiotherapist tries to accelerate the orthosis and the teaching-in device by 5 [N], but only 2 [N] will actually accelerate the structure, while 3 [N] will act against the resistance of the robotic arm. These values are tolerable compared to the total force $\hat{F}$ (see Figure 2) up to the range of 100 [N], which accelerates the total arm of the patient.

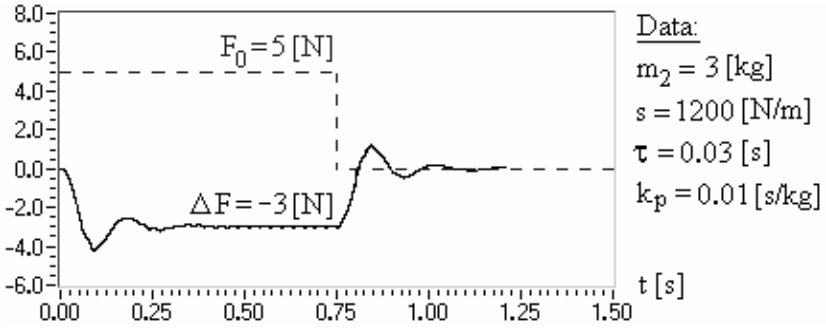

Figure 9 Numerical simulation results at specified parameters

Figure 10 presents the simulated self excited vibration of the robot at the loss of stability when the same dimensionless frequency $\gamma = 0.6$ is used as above, but the proportional gain k_p is just higher than the stability limit in (39). Figure 8 gives the dimensionless frequency $\omega = 1.239$, which gives a vibration frequency

$$f = \omega/(2\pi\tau) = 6.575\ [\mathrm{Hz}] \ . \tag{41}$$

This corresponds perfectly to the time period $T = 1/f = 0.152$ [s] of the simulated self-excited oscillation shown in Figure 10.

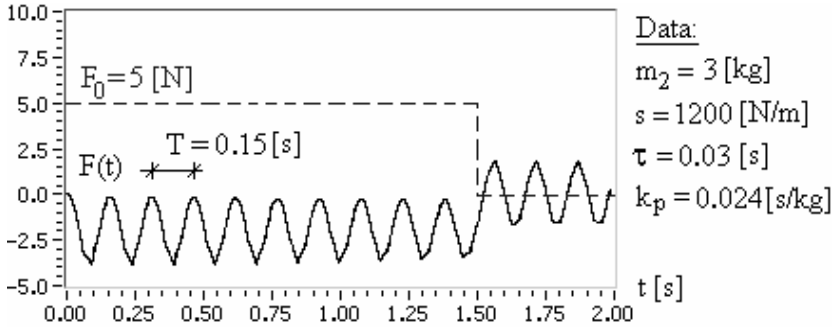

Figure 10 Numerical simulation of the Neimark-Sacker bifurcation

7 Conclusions

This paper described a simplified model for the teaching-in process of standard industrial robots with standard F/T sensors. In compliance with other authors Lange and Hirzinger [18], Dessen, F. and Balchen J.G. [19] it was observed that a low stiffness spring in the teaching-in device makes the control stable. In contrast with other approaches, there is no need here to include new or alter elements in the system as the electromechanical safety relaxer presents very low stiffness.

The results clearly show the strong limitations caused by the relatively low sampling rate of the industrial robot, and the necessity of the delicate design of the mechanical and control parameters to achieve the goal of the REHAROB project – or the goal of any teaching-in method via force control. The results also explain why the robots oscillate with low frequency relative to the sampling frequency of the digital control in case of unstable parameter settings.

Before the control strategy is applied and extended for real industrial ABB robots, we checked the performance of the system by numerical simulation. The numerical results confirmed the predicted stability behaviour and the estimated resistance of the robot during teaching-in via digital force control (see Figure 9 and 10).

Further research is required to extend the technology into 6 DOF, and to implement the control algorithm in RAPID programming environment of ABB industrial robots.

Acknowledgement

This work was supported by the IST-1999-13109 REHAROB project of the 5th Framework Programme of the European Union, and the Hungarian Scientific Research Foundation under grant No. OTKA T030762.

References

[1] Hogan, N.; Kerbs, H.I.; Charnnarong, J.; Srikrishna, P.; Sharon, A.: MIT-MANUS: a workstation for manual therapy and training II. Proc Teleman Tech –SPIE: Intl Soc Optical Eng, 1833, Nov. 1992.

[2] Lum, P.S.; Van der Loos, M.; Shor, P.; Burgar, C.G.: A robotic system for upper limb exercises to promote recovery of motor function following stroke, ICORR'99, pp235-239, 1999.

[3] Ramathan, R.; Stroud, S.; Alexander, M. (1995) Powered orthosis project forum, ASEL Technical Report #ROB9405, Applied Science & Engineering Laboratories, University of Delaware/A.I. duPont Institute, 1600 Rockland Rd., P.O. Box 269, Wilmington DE 19803.

[4] Interactive Motion Technologies Inc., 56 Highland Avenue, Cambridge, Mass. 02139, US http://interactive-motion.com

[5] Hogan, N.; Kerbs, H.I.; Sharon, A; Charnnarong, J.: U.S. Patent 5,466,213; Massachusetts Institute of Technology, 1995.

[6] Harwin, W.S.: Design of an active arm support for assisting arm movements, Advances in manufacturing: decision, control and information technology / [edited by] S.G. Tzafestas, Selected papers from the 3rd European Robotics, Intelligent Systems and Control Conference (EURISCON'98), Athens, Greece, June 22-25, 1998, Springer-Verlag, p. 233-244.

[7] Harwin, W.S.: Analysis of force-reflecting telerobotic systems for rehabilitation applications, Proceedings of the 1st European Conference on Disability, Virtual Reality and Associated Technologies pp 171-178, ISBN 07049 1140X (1996).

[8] Johnson, G.R.; Valeggi, R.; Parrini, G.; et al.: MULOS – A new motorized upper limb orthoic system. Proceeding of the 9th Word Congress, International Society of Prosthetics and Orthotics, Amsterdam, June 28 – July 3 1998, p639.

[9] Raibert, M. H.; Craig, J.J.: Hybrid position force control for computer controlled manipulators. ASME J. Dynamics Systems, Measurement and Control 102 (1981), 125-133.

[10] Craig, J.J.: Introduction to robotics mechanics and control. Addison-Wisley, Reading 1986.

[11] Whitney, D.E.; Force feedback control of manipulator fine motions, ASME Journal of Dynamics Systems, Measurement and Control 98, 1977, pp.91-97.

[12] Whitney. D.E.: Historical perspective and state of the art in robot force control, International Journal of Robotics Research 6, 1985, pp.3-17.

[13] Stépán, G.; Haller, G.: Quasiperiodic Oscillations in Robot Dynamics, Nonlinear Dynamics, vol. 8 (1995), pp. 513-528.

[14] Haller, G., Stépán, G., 1996 Micro-chaos in digital control, *J. of Nonlinear Science* 6 pp. 415-448.
[15] Stépán, G.: Vibrations of Machines Subjected to Digital Force Control, International Journal of Solids and Structures, vol. 38 (2001), pp. 2149-2159.
[16] Kuo, B.C., 1977. Digital Control Systems. SRL Publishing Company, Champaign, Illinois.
[17] Farkas, M., 1994. Periodic Motions. Springer, New York.
[18] Lange, F.; Hirzinger, G.: Learning Force Control with Position Controlled Robots, 1996 IEEE International Conference on Robotics and Automation, Minneapolis, April 1996.
[19] Dessen, F.; Balchen, J.G.: Fast Sensory Control of Robot Manipulators, NATO ASI Series, Vol. F63 Traditional and Non-traditional Robotic Sensors edited by T. C. Henderson, Springer-Verlag Berlin Heidelberg 1990.